EXPLOSION MODELS, LIGHT CURVES, SPECTRA AND H_O

P. HÖFLICH
Harvard University, Center for Astrophysics
60 Garden Str., Cambridge, MA 02138, USA

A. KHOKHLOV AND J.C. WHEELER
Dept. of Astronomy, U. of Texas, Austin, TX78712, USA

K. NOMOTO
Dept. of Astronomy, U. of Tokyo 113, Japan

AND

F.K. THIELEMANN
Depart. of Physics, U. Basel, Klingelberg-Str. 62, Switzerland

Abstract. From the spectra and light curves it is clear that SNIa events are thermonuclear explosions of white dwarfs. However, details of the explosion are highly under debate. Here, we present detailed models which are consistent with respect to the explosion mechanism, the optical and infrared light curves (LC), and the spectral evolution. This leaves the description of the burning front and the structure of the white dwarf as the only free parameters. The explosions are calculated using one-dimensional Lagrangian codes including nuclear networks. Subsequently, optical and IR-LCs are constructed. Detailed NLTE-spectra are computed for several instants of time using the density, chemical and luminosity structure resulting from the LCs. The general methods and critical tests are presented (sect. 2).

Different models for the thermonuclear explosion are discussed including detonations, deflagrations, delayed detonations, pulsating delayed detonations (PDD) and helium detonations (sect.3). Comparisons between theoretical and observed LCs and spectra provide an insight into details of the explosion and nature of the progenitor stars (sect. 4 & 5). We try to answer several related questions. Are subluminous SNe Ia a group different from 'normal' SN Ia (sect. 5)? Can we understand observed properties of the LCs and spectra (sect. 4)? What do we learn about the progenitor evolution and its metallicity (sect. 3, Figs. 4,5)? Do successful SN Ia models depend on the type of the host galaxy (Table 2)?

Using both the spectral and LC information, theoretical models allow for a determination of the Hubble constant independent from 'local' distance indicators such as δ Cephei stars. H_o is found to be $67 \pm\ 9\ km\ s^{-1} Mpc^{-1}$ and, from SN1988U, q_o equals $0.7 \pm 1.$ within 95 % confidence levels.

1. Introduction

During the last few years it became evident that Type Ia supernovae are a less homogeneous class than previously believed (e.g. Barbon et al., 1990, Pskovskii 1970, Phillips et al. 1987). In particular, the observation of subluminous SN1991bg (Fillipenko et al. 1992, Leibundgut et al. 1993) raised questions on the SN-rate and whether we have missed a huge subgroup. The possible impact on our understanding of supernovae statistics and, consequently, the chemical evolution of galaxies must be noted.

It is generally accepted that SNe Ia are thermonuclear explosions of carbon-oxygen white dwarfs (WD) (Hoyle & Fowler 1960). However, details of the scenario are still under debate. For discussions of various theoretical aspects see e.g. Wheeler & Harkness (1990), Woosley & Weaver (1994), Canal (1995), Nomoto et al. (1995), Wheeler et al. (1995).

What we observe as a supernovae event is not the explosion itself but the light emitted from a rapidly expanding envelope produced by the stellar explosion. As the photosphere recedes, deeper layers of the ejecta become visible. A detailed analysis of the LCs and spectra gives us the opportunity to determine the density, velocity and composition structure of the ejecta. A successful application of these constraints, however, requires both accurate early LC and spectral observations and detailed theoretical models. While SN Ia LC data have enormously increased, until recently (Harkness 1991; Höflich et al. 1991), models are often hampered by inadequate physical assumptions like a constant opacity, crude gamma-ray deposition schemes and a simplified treatment of the ionization balance, neglect of line scattering and by the use of the diffusion approximation (e.g. Livne & Arnett 1995). Based on our detailed models which overcome the approximations just mentioned, we have investigated the validity and influence of the physical assumptions made in LC and spectral calculations and estimated the accuracy of our models. The importance of a consistent treatment of the explosion mechanism, LCs and spectra became evident. Some of the tests and the basic outline of our approach is given in section 2. In section 3, the basic explosion mechanism are discussed. After investigating the general properties of our LCs and spectra, individual comparisons with observations are presented. Finally, we address the question on H_o and q_o.

2. Brief Description of the Numerical Methods

2.1. HYDRODYNAMICS

The explosions are calculated using one-dimensional Lagrangian hydro with artificial viscosity (Khokhlov, 1991ab) and radiation-hydro codes including nuclear networks (Höflich & Khokhlov 1995). The latter code is based on our LC code that solves the hydrodynamical equations explicitly by the piecewise parabolic method (Collela and Woodward 1984) and includes the solution of the radiation transport implicitly via the moment equations, expansion opacities, and a detailed equation of state. Typically, 300 to 500 depth points are used. Radiation transport has been included to provide a smoother transition from the hydrodynamical explosion to the phase of free expansion. We omit γ-ray transport during the hydrodynamical phase because of the high optical depth of the inner layers. Nuclear burning is taken into account using Thielemann's network (Thielemann, Nomoto & Hashimoto 1994 and references therein). During the hydro, an α-network of 20 isotopes is considered to properly describe the energy release. Based on a network of 216 isotopes, the final chemical structure is calculated by postprocessing the hydrodynamical model. The accuracy of the energy release has been found to be about 1 to 3 % in the reduced network compared to about 15 % for the equation net work used previously (Khokhlov, 1991) which, in general, overestimate the expansion velocity accordingly.

2.2. LIGHT CURVES

Based on the explosion models, further hydrodynamical evolution, and bolometric and monochromatic light curves are calculated using a scheme recently developed and widely applied to SN Ia (Höflich et al. 1995 and references therein). In principle, it is the same code as that described above, but nuclear burning is neglected and γ ray transport is included via a Monte Carlo scheme. In order to allow for a more consistent treatment of scattering, we solve both the (two lowest) time-dependent radiation moment equations for the radiation energy and the radiation flux, and a total energy equation (Mihalas 1978). The Eddington factors are obtained by formal integration of the radiation transport equation. The opacities have been calculated under the assumption of local thermodynamical equilibrium. This is a reasonable approximation since diffusion time scales are governed by layers of large optical depth. The Planck and the Rossland mean of the absorption opacity and extinction, respectively, have been calculated based on an approach similar to Karp et al. (1977) but transformed to the comoving frame. Relativistic terms are neglected. As in any Sobolev approach, it is assumed that the resonance region of lines is small. Therefore, the mean

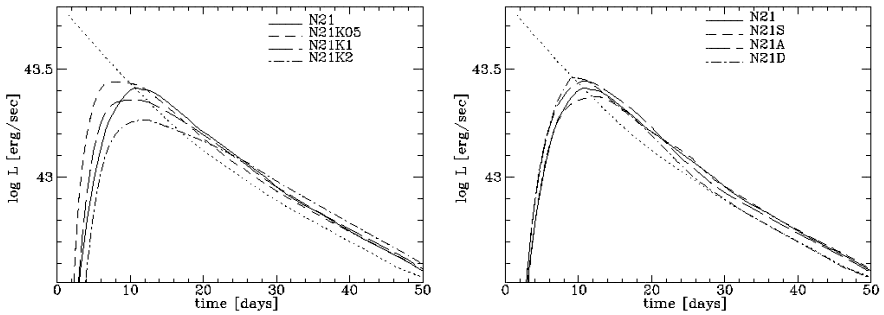

Figure 1. Bolometric LC of the delayed detonation model N21 for various assumptions (N21: all effects are included as described in the text; N21K2, N21K1 & N21K05: $\kappa_R = \kappa_P = const$ with 0.20, 0.1 and 0.05 cm^2/g, respectively; N21S: $\kappa_P = \kappa_R$, N21A; extinction = true absorption; N21D: diffusion approximation). In addition the energy release due to the radioactive decay of ^{56}Ni and ^{56}Co is shown (dotted line). If constant opacities are assumed, explosion models cannot be tested because the strong temperature dependence of the opacity for $T \leq 20000K$ is neglected. This effect determines the shape of LCs near maximum light. For reasonable variations in κ (Shigeyama et al. 1993), the time of maximum light is shifted by up to 5 days and the maximum brightness may be off by about 50% . The shape of the LCs differ strongly. If the temperature dependence of the opacity is included, the spread in the results shrinks to about 20 % both with respect to the rise time and absolute flux. The slope becomes comparable within 10% if the radiation transport equation is solved rather than assuming the diffusion approximation.

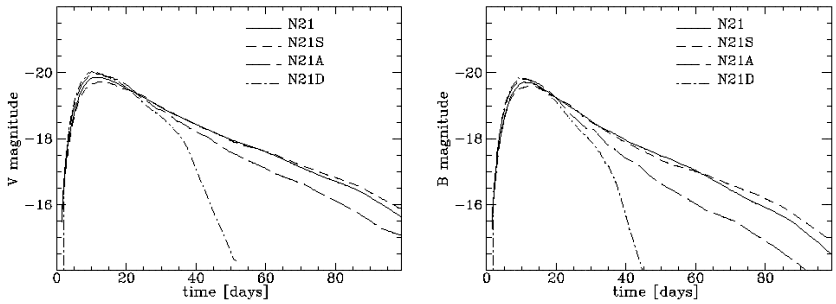

Figure 2. B and V LCs of N21 for various assumptions (see Fig. 1). Apparently, both the diffusion approximation (N21D) and the neglection of line scattering (extinction = true absorption, N21A) are inadequate. The the local cooling of the radiaton field is strongly overestimated since, in SNeIa, scattering exceeds the true absorption by a factor of 100 to 10000 (Höflich et al. 1993, Höflich 1995). In comparison, the corresponding error by setting $\kappa_R * \alpha = \kappa_P$ in the energy equations results in errors of about 0.1 m because the thermal coupling differs by a much smaller factor (≈ 5 ... 10). The surprisingly small sensitivity of the resulting LCs can be understood in terms of the energy conservation. Namely, during early times, the energy balance is determined by radioactive decay and the adiabatic expansion if the opacity exceeds a certain limit.

free path of a photon along a certain ray is given by the product of inverse absorption probabilities weighted with the absorption probabilty of transi-

tions being closer to the comoving frame wavelength. The expansion effect enters both the Planck and the Rosseland mean but the former in second order, only, because the Planck mean is a linear average of κ_ν. The main problem with the Planck opacity is related to line scattering. In SNeIa, scattering exceeds true absorption by several orders of magnitude. Therefore, scattering must be included. Since 1993, we have used an equivalent-two level approach calibrated by detailed NLTE-calculations (see below, Höflich 1995). We found that the thermalization process is governed by redistribution (i.e. collisions) of energy within the atomic fine structure levels and not by the scattering in about a dozen UV lines (Pinto, talk at this meeting). The former effect is dominant since collisional cross sections depend exponentially on the energy difference between levels. In fact, the two-level approach underestimates the size of the thermalization by several orders of magnitude as it is well known in the field of stellar atmospheres (e.g Mihalas 1978, Ayres 1989). For details, see Höflich (1995).

Monochromatic colors B, V, R, and I are calculated using 100 discrete wavelength bands and formal integration along rays. For several models, detailed NLTE-spectra have been constructed (Höflich, 1995). The colors based on the NLTE atmospheres and LC calculations have been compared. Typically, the disagreements between these two techniques in V, B, R, and I are below 0.05 to 0.1^m near maximum light and remain between 0.2 to 0.4^m at late time. The error is small because most lines are scattering dominated. Consequently, the flux is redistributed within a wavelength range corresponding to the Doppler shift produced by the photospheric expanson. However, this frequency shift is small compared to the bandwidth of the UBVRI-filter. With increasing time, the forbidden lines dominate the flux and, consequently, the error in our monochromatic colors increases. Another uncertainty when comparing with observations is due to the filter functions. Here, we use transmission functions given by Bessell (1990).

In light of the uncertainties, we have compared our opacities with those based on approximations by Jeffery (1995). We found good agreement. Moreover, the sensitivity of the resulting LCs variations in the uncertain quantities have been studied in great detail (Höflich et al. 1993, Khokhlov et al. 1994). Some of the results are shown in Figs. 1 and 2. Other, independent tests are provided by the comparisons with observations. We find that our bolometric correction is consistent with the observation of SN1992A, and the distances predicted by our models agree with those based on δ-Ceph stars in IC4182, NGC5253 and 4536 (Höflich & Khokhlov 1995). The former test probes the overall energy distribution, whereas the latter test is sensitive to errors in the absolute, monochromatic fluxes.

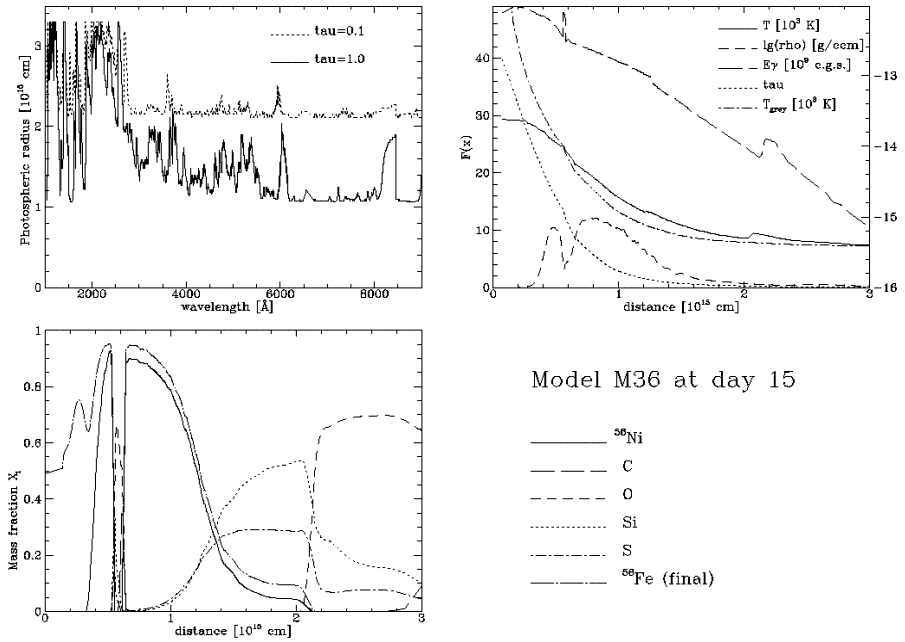

Figure 3. Various quantities for M36 15 days after the explosion. Distances are given as a function of wavelength at which the monochromatic optical depth reaches 0.1 and 1, respectively (upper left), Temperature T, density ρ, energy deposition due to radioactive decay E_γ and Rosseland optical depth are given as a function of distance and, for comparison, T_{grey} for the grey extended atmosphere (upper right), and chemical profile are presented for the most abundant elements (lower left). No well defined photosphere exists. The need for spectral analyses consistent with respect to the explosion mechanism, $\gamma-$ray transport and LC calculation is obvious. Already at maximum light, the chemical distribution of elements does not follow the density profile but shows large individual variations in the line forming region, i.e. between 1 and 2 10^{15} cm. The smallest expansion velocity indicated by line shifts are predominantly determined by the chemical profiles and not by the density. The energy deposition and excitation due to γ-rays becomes important within the photosphere. Consequently, the luminosity cannot be assumed to be depth independent for the construction of synthetic spectra.

2.3. SYNTHETIC SPECTRA

A modified version of our code for Nlte Extended ATmospheres (NEAT) is used. For details see Höflich (1990, 1995) and references therein.

Stationarity is assumed where the density, chemical profiles and the luminosity as a function of the radial distance r are given by results of the hydrodynamical explosion and of the LC calculations including the Monte-Carlo scheme for the γ-ray transport (Fig. 3).

The radiation transport equation is solved in the comoving frame including relativistic terms. For the determination of the first moment of the intensity, we solve the radiation transport equation for strong lines includ-

ing 'quasi' continua (weak lines are treated in a Sololev approximation, see below) in the comoving frame, i.e.

$$Op\ I = \chi(S - I)$$

$$I = I(\mu, r, \nu); \qquad S = S(r, \nu); \qquad \chi = \chi(r, \nu)$$

(μ: cosine between the radial direction and I; r : radial distance; v(r) : radial velocity; S: source function; χ: absorption coefficient; ν: frequency). The operator Op can be written as follows (Castor, 1974):

$$Op = \left[\mu + \frac{v(r)}{c}\right]\frac{\partial}{\partial r} + \left[\frac{(1-\mu^2)}{r}\Big(1 + \frac{\mu v(r)}{c}(1 - \beta(r))\Big)\right]\frac{\partial}{\partial \mu}$$

$$-\left[\frac{v(r)\nu}{c \cdot r}\Big(1 - \mu^2 + \mu^2\beta(r)\Big)\right]\frac{\partial}{\partial \nu} + \left[\frac{3v(r)}{c \cdot r}\Big(1 - \mu^2 + \beta(r)\mu^2\Big)\right]$$

with

$$\beta := \frac{d\ ln\ v(r)}{d\ ln\ r}.$$

The term in front of $\frac{\partial}{\partial \nu}$ can be interpreted as the classical Doppler shift. The second terms of the partial derivatives with respect to r, μ and the logarithmic derivative of v(r) correspond to the advection and aberration effects. For practical purpose, we solve the non relativistic transport equation using a Rybicki scheme (Mihalas et al., 1975, 1976). Overlapping lines in the comoving frame cannot be treated because the system is solved as a boundary problem in the frequency space which, from the concept, disallows a propagation of information toward higher/lower frequencies for expanding/collapsing envelopes. The same limitation should also apply to Nugent et al. (1995a) who use the same method. However, the problem of overlapping lines can be and has been solved (Höflich 1990) in full analogy with the problem of partial redistribution using a Fourtrier-like scheme (Mihalas et al, 1976b). Although our code can deal with partial redistribution, this effect is neglected to save CPU-time. A technical problem is the fact that each line must be sampled by at least 10 frequency points to provide a sufficient accurate representation of the $\delta/\delta\nu$-term (Mihalas et al. 1975). Therefore, we must limit this approach to ≈ 2000 lines.

Blocking by lines other than the strong ones is included in a 'quasi' continuum approximation, i.e. the frequency derivative terms in the radiation transport equation is included in the narrow line limit to calculate the probability for photons to pass a radial sub-shell along a given direction μ (Castor, 1974, Abbot and Lucy 1985, Höflich, 1990). Note that the information on the exact location of the interaction within a subshell gets lost translating into an uncertainty in the wavelength location of $\approx 10^{-3}$.

The statistical equations are solved consistently with the radiation transport equation to determine the non-LTE occupation numbers using both an accelerated lambda iteration (see Olson et al. 1986) and an equivalent-two level approach for transitions from the ground state which provides an efficient way to take the non-thermal fraction of the source function into account during the radiation transport and, effectively, accelerate both the convergence rate and the stability of the system. A comparison of the explicit with the implicit source functions provides a sensitive tool to test for convergence of the system of rate and radiation transport equations.

Excitation by gamma rays is included. Detailed atomic models are used for up to three most abundant ionization stages of several elements, i.e. (He), C, O, Ne, Na, Mg, Si, S, Ca, Fe taking into account 20 to 30 levels and 80 - 150 transitions in the main ionization stage. Here, we use detailed term-schemes for C II, O II, Ne I, Na I, Mg II, Si II, S II, Ca II and Fe II or Fe III. The corresponding lower and upper ions are represented by the ground states. The energy levels and cross sections of bound-bound transitions are taken from Kurucz (1993). In addition to our NLTE-transitions, a total of $\approx 300,000$ lines out of a list of 31,000,000 (Kurucz, 1993) are included for the radiation transport. For these lines, we assume LTE population numbers inside each ion. To calculate the ionization balance, excitation by hard radiation is taken into account. LTE-line scattering is included using an equivalent-two-level approach calibrated by our NLTE-elements.

3. Hydrodynamical Models

3.1. EXPLOSIONS OF MASSIVE WHITE DWARFS

A first group consists of massive carbon-oxygen white dwarfs (WDs) with a mass close to the Chandrasekhar mass which accrete mass through Roche-lobe overflow from an evolved companion star (Nomoto & Sugimoto 1977; Nomoto 1982). The explosion is triggered by compressional heating. The key question is how the flame propagates through the white dwarf. Several models of SNeIa have been proposed in the past, including detonation (Arnett 1969; Hansen & Wheeler 1969), deflagration (e.g. Nomoto, Sugimoto & Neo 1976) and the delayed detonation model, which assumes that the flame starts as a deflagration and turns into a detonation later on (Khokhlov 1991, Woosley & Weaver 1995, Yamaoka et al. 1992).

Our sample includes detonations (DET1/2), deflagrations (W7, DF1, DF1mix), delayed detonations (N21/32, M35-39; DD13-27) and pulsating delayed detonations (PDD1-9). The deflagration speed is parameterized as $D_{def} = \alpha a_s$, where a_s is the local sound velocity ahead of the flame and α is a free parameter. The speed of the detonation wave is given by the sound-speed behind the front. For delayed detonation models, the transition to a

TABLE 1. Some quantities (see text) are given for detonations (DET1/DET2, asterix), deflagrations (W7, DF1, DF1mix, circles), delayed detonations (N21, N32, M35-M312, DD13c - 27c, bullets), pulsating delayed detonations (PDD1a-9, black triangles), envelope models (DET2env2/4, open triangles), and helium detonations (HeD2-12, open asterix). The C/O ratio has been assumed to be 1:1 unless otherwise quoted in brackets after the name. The initial metallicity for $Z \geq 20$ is assumed to be solar, but for DD24c, DD25c, DD26c and DD27c for which 1/3, 3, 0.1 and 10 times solar abundances are used, respectively. Otherwise, these models are identical to DD21c. For the helium detonations and envelope models, the mass is of the C/O core, and of the He-layers or of the extended CO-envelope, respectively, are given separately. In HeD7, no central C-ignition is triggered.

Model	$M_\star$ $[M_\odot]$	ρ_c $[10^9 c.g.s]$	α	ρ_{tr} $[10^7 c.g.s]$	E_{kin} $[10^{51} erg]$	M_{Ni} $[M_\odot]$
DET1	1.4	3.5	—	—	1.75	0.92
DF1	1.4	3.5	0.30	—	1.10	0.50
W7	1.4	2.0	n.a.	—	1.30	0.59
N21	1.4	3.5	0.03	5.0	1.63	0.83
N32	1.4	3.5	0.03	2.6	1.52	0.56
M35	1.4	2.8	0.03	3.0	1.56	0.67
M36	1.4	2.8	0.03	2.4	1.52	0.60
M37	1.4	2.8	0.03	2.0	1.49	0.51
M38	1.4	2.8	0.03	1.7	1.44	0.43
M39	1.4	2.8	0.03	1.4	1.38	0.34
M312	1.4	2.8	0.03	1.0	1.35	0.20
DD13c (1:1)	1.4	2.6	0.03	3.0	1.36	0.79
DD14c (1:2)	1.4	2.6	0.03	3.0	1.21	0.79
DD15c (2:3)	1.4	2.6	0.03	3.0	1.28	0.79
DD21c (1:1)	1.4	2.6	0.03	2.7	1.32	0.69
DD23c (2:3)	1.4	2.6	0.03	2.7	1.18	0.59
PDD3	1.4	2.1	0.04	2.0	1.37	0.49
PDD5	1.4	2.7	0.03	0.76	1.23	0.12
PDD8	1.4	2.7	0.03	0.85	1.30	0.18
PDD7	1.4	2.7	0.03	1.1	1.40	0.36
PDD9	1.4	2.7	0.03	1.7	1.49	0.66
PDD6	1.4	2.7	0.03	2.2	1.49	0.56
PDD1a	1.4	2.4	0.03	2.3	1.65	0.61
PDD1c	1.4	2.4	0.03	0.71	0.47	0.10
HeD2	0.6+0.22	.013	—	—	0.94	0.43
HeD4	1.0+0.18	.150	—	—	1.50	1.07
HeD6	0.6+0.172	.0091	—	—	0.72	0.252
HeD7	0.6+0.14	.0089	—	—	—-	—-
HeD8	0.8+0.16	.025	—	—	1.08	0.526
HeD10	0.8+0.22	.036	—	—	1.24	0.75
HeD11	0.9+0.16	.061	—	—	1.37	0.87
HeD12	0.9+0.22	.083	—	—	1.45	0.92
DET2	1.2	0.04	—	—	1.52	0.63
DET2env2	1.2 + 0.2	0.04	—	—	1.52	0.63
DET2env4	1.2 + 0.4	0.04	—	—	1.52	0.63
DET2env6	1.2 + 0.6	0.04	—	—	1.52	0.63

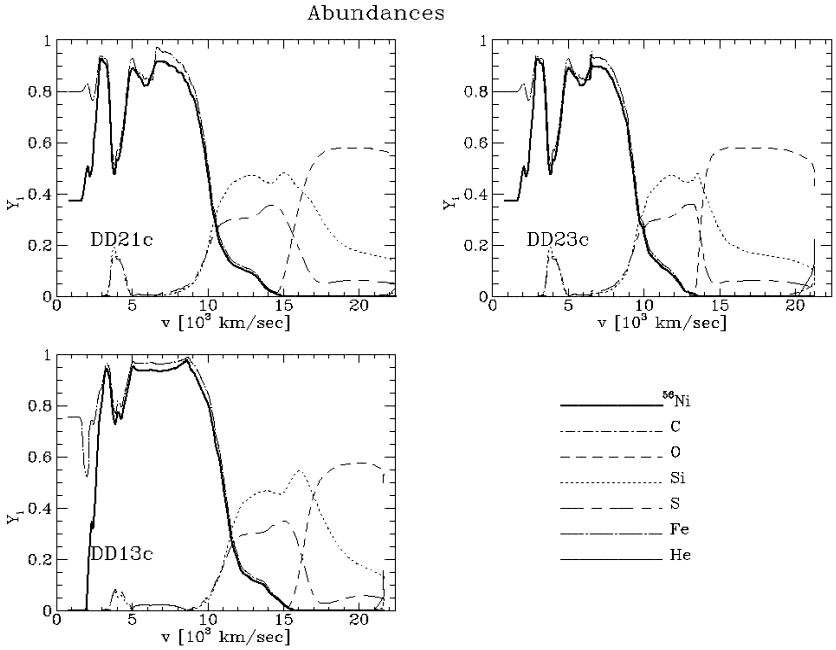

Figure 4. Abundances as a function of the expansion velocity for three delayed detonation models (see table 1). Since the burning time scales to NSE or partial NSE are shorter than the hydrodynamical time scales for all but the very outer layers, the final products depend mainly on the density at which burning takes place. With decreasing transition density, lesser ^{56}Ni is produced and the intermediate mass elements expand at lower velocities because the later transition to a detonation allows for a longer pre-expansion of the outer layers (DD21c vs. DD13c). Similarily, with increasing C/O ratio in the progenitor, the specific energy release during the nuclear burning is reduced (DD23c vs. DD21c) and the transition density at the burning front reached later in time, resulting in a larger preexpansion of the outer layers. This may allow to determine the main sequence mass of the progenitor.

detonation is given by another free parameter ρ_{tr}. When the density ahead of the deflagration front reaches ρ_{tr}, the transition to a detonation is forced by increasing α to 0.5 over 5 time steps bringing the speed well above the Chapman-Jouguet theshold for steady deflagration. For pulsating delayed detonation models, the initial phase of burning fails to release sufficient energy to disrupt the WD. During the subsequent contraction phase, compression of the mixed layer of products of burning and C/O formed at the dead deflagration front would give rise to a detonation via compression and spontaneous ignition (Khokhlov 1991). In this scenario, ρ_{tr} represents the density at which the detonation is initiated after the burning front dies out. Besides the description of the burning front, the central density of the WD at the time of the explosion is another free parameter. For white dwarfs close to the Chandrasekhar limit, it depends sensitively on the chemistry and the accretion rate $\dot{M}$ at the time of the explosion. In our recent study

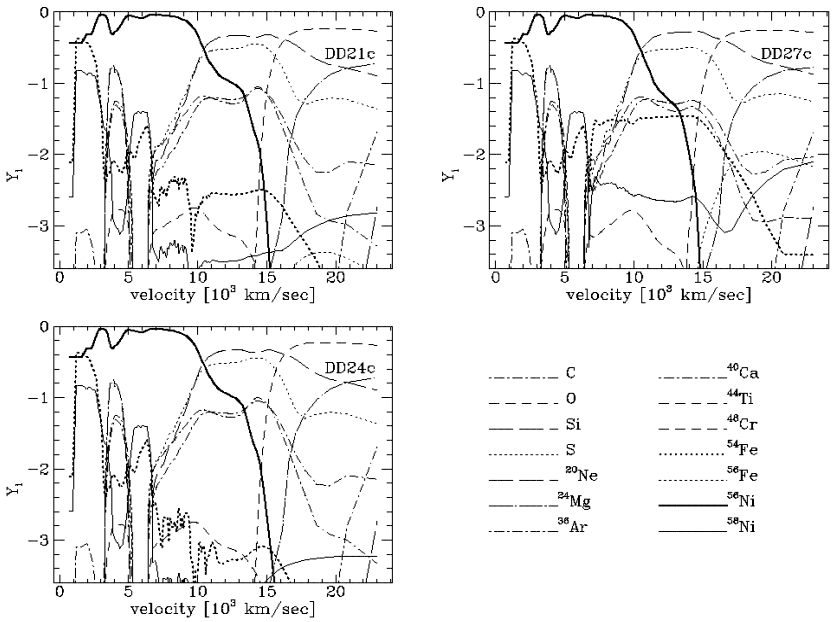

Figure 5. Abundances for three delayed detonation models (DD21c, DD24c & DD27c) with identical parameters but different initial metallicity (Z $\geq$ 20) corresponding to 1, 1/3 and 10 times solar. The overall density, velocity and chemical structure remains uneffected but the isotopic composition changes drastically. In particular, the final *Fe* abundance differ by more than two orders of magnitude in the outer layers and may be as high as 7 % which clearly shows up in synthetic spectra. Whether this provides a natural explanation of the spectral peculiarities of SN1991T is under investigation.

on SN1994D, evidence was found that the models with a somewhat smaller central density provide better agreement with both the observed spectra and LCs. Therefore, the grid of PDD models has been extended.

3.2. MERGING WHITE DWARFS

The second group of progenitor models consists of two low-mass white dwarfs in a close orbit which decays due to the emission of gravitational radiation and this, eventually, leads to the merging of the two WDs (e.g. Iben & Tutukov 1984). After the initial merging process, one low density WD is surrounded by an extended envelope (Hachisu, Eriguchi & Nomoto 1986ab, Benz, Thielemann & Hills 1989). This scenario is mimicked by our envelope models DET2env2...6 in which we consider the detonation in a low mass WD surrounded by a compact envelope between 0.2 and 0.6 $M_\odot$.

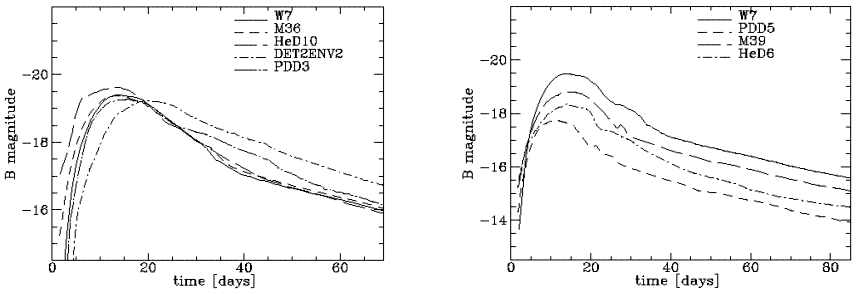

Figure 6. Monochromatic V LCs of normal bright supernovae of deflagration (W7), classical delayed detonation (M36), Helium detonation (HeD10), envelope (DET2env2), pulsating delayed detonation (PDD3) models, and of subluminous SNeIa classical delayed detonation (M39), Helium detonation (HeD6), pulsating delayed detonations(PDD5).

3.3. EXPLOSIONS OF SUB-CHANDRASEKHAR MASS WHITE DWARFS

Another class of models – double detonation of a C/O-WD triggered by detonation of helium layer in low-mass WDs – was explored by Nomoto (1980), Woosley & Weaver (1980), and most recently by Woosley and Weaver (1994, hereafter WW94) and Höflich & Khokhlov (1995). This scenario was also suggested for the explanation of subluminous Type Ia (WW94). Note that the explosion of a low mass WD was also suggested by Ruiz-Lapuente et al. (1993) to explain subluminous SNe Ia but the mechanism for triggering of the central carbon detonation was not considered.

For ease of comparison, we have used parameters close to those suggested in WW94. To prevent repetition, we refer to the latter work for a detailed discussion of this class of models. Helium detonations show a qualitatively different structure in comparison to all models with a Chandrasekhar mass WD . The intermediate mass elements are sandwiched by Ni and He/Ni rich layers at the inner and outer regions, respectively. Generally, the density smoothly decreases with mass because partial burning produces almost the same amount of kinetic energy as the total burning, but a moderate shell-like structure is formed just below the former Helium layers. Observationally, a distinguishing feature of this scenario is the presence of Helium and Ni with expansion velocities above 11,000 to 14,000 $km\ s^{-1}$. Typically 0.07 to 0.13 $M_\odot$ of Ni are produced in the outer layers, mainly depending on the mass of the Helium shell. Recently, Benz (1995, private communication) suggested that the explosion of the C/O core may be triggered directly by the in-going shock front if Helium is ignited somewhat above the He/C-O interface. This, however, should hardly change the chemical structure because the flame propagates as a detonation.

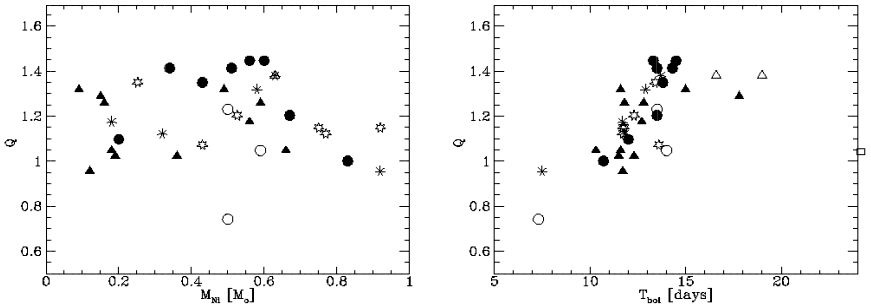

Figure 7. Ratio Q between the bolometric luminosity and the energy release by gamma decay at t_{bol} as a function of the ^{56}Ni mass (left) and rise time to bolometric maximum t_{bol}. The different symbols correspond to different explosion scenarios (see Table 1).

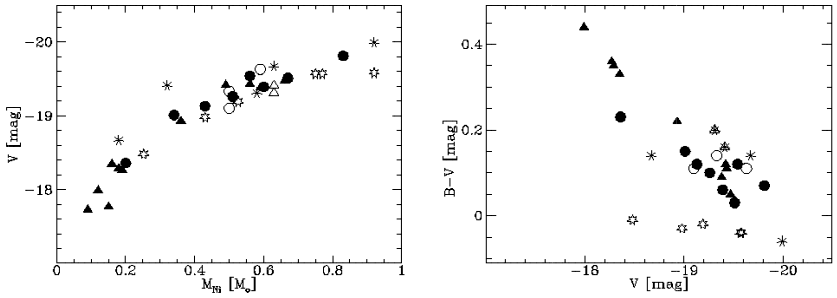

Figure 8. Absolute visual brightness V as a function of the ^{56}Ni mass (left) and intrinsic color B-V as a function of V(right).

4. Comparison with Observations

The different explosion scenarios can generally be distinguished based on differences in the slopes of the early monochromatic LCs (Fig. 6) and the expansion velocities indicated by the spectra (Fig. 9 & Höflich, this volume). For all models with a ^{56}Ni production $\geq 0.4 M_\odot$, M_V ranges from -19.1 to -19.7^m. As a general tendency, the post-maximum declines are related to M_V, but there is a significant spread in the decline rate among models with similar brightess. For all models but the Helium detonations, the colors become very red for small M_{Ni} (Fig. 8).

As a general trend, the maxima of subluminous supernovae are more pronounced. The reason becomes obvious if we consider the following related point. In the literature (Arnett et al. 1985), it is often assumed that the bolometric luminosity L_{bol} is equal to the instantaneous release of energy by radioactive decay L_γ, i.e. $Q = L_{bol}/\dot{E}_\gamma \approx 1$, independent from the model. We find that Q depends on the model because the opacities vary

strongly with temperature. Typically, Q ranges from 0.7 to 1.4 (Fig. 7). For models with fast rising LCs, the opacity stays high and the photosphere recedes mainly by the geometrical dilution of matter. For models with a slower rise time or little ^{56}Ni, the opacity drops strongly at about maximum light. The photosphere receds quickly in mass, and thermal energy can be released from a larger region. Because no additional energy is gained, the energy reservoir is exhausted faster, and the post-maximum decline becomes steeper.

The distinguishing features of Helium detonations are blue maxima both for normal and subluminous supernovae, a rapid increase of the luminosity caused by ^{56}Ni heating, followed by a phase of slow rise to maximum light and a fast post-maximum decline. The fast decline is caused by the rapid increase of the escape probability of γ photons originating in the outer ^{56}Ni and the short life time of ^{56}Ni. The early synthetic spectra are dominated by high velocity Ni and the absence of Si which is underabundant by more than two orders of magnitude compared to delayed detonation models. Note that a significant amount of the line emission at late phases should be powered by ^{56}Co at high velocities. In the subluminous models, about 1/2 to 1/4 of the radioactive material is ejected at high velocities. Accordingly, late-time spectra should show broad Co and Fe lines.

5. Comparison between Observation and Models Predictions

We use a quantitative method for fitting data to models based on Wiener filtering (Rybicki and Press, 1995). The reconstruction technique is applied to the standard deviation from the theoretical LC to avoid problems with measurements distributed unevenly in time. By minimizing the error, the time of the explosion, the distance, and the reddening correction can be determined. For details, see Höflich & Khokhlov (1995).

Observed monochromatic LCs and spectra of 27 SNe Ia are compared with theoretical models (Table 2, Fig. 9 & Höflich, this volume). According to our results, normal bright, fast SNeIa (e.g. SN 1971G, SN 1994D) with rise times up to 15 days (17 days) for the blue (visual) LC can be explained by delayed detonation with different densities ρ_{tr} for the transition from a deflagration to a detonation. For PDDs, the density ρ_{tr} stands for the density at which the detonation starts after the first pulsation. Typically, ρ_{tr} is about 2.5 10^7 $g\ cm^{-3}$. Central densities of the initial WDs range from 2.1 to 3.5 $10^9 g\ cm^{-3}$. As a tendency, models at the lower end of this range tend to give somewhat better fits. This may be explained by a high accretion rate, some variation in the chemical composition or by an additional trigger mechanism for the explosion. We note that the classical deflagration W7 (Nomoto et al. 1984) provides similar good fits in several

TABLE 2. List of observed SNeIa used in our sample. Columns 2 to 7 give the parent galaxy, its type, peculiar velocity v_z according to the MERCG catalogue (Kogoshvili 1986), the distance modulus of the host galaxy and the color excess E_{B-V} of the SNe Ia as determined from our models. In column 8, we give names of those theoretical models (see Table 1) which can reproduce the observed LCs. Models in bracketts do not fullfil our criterion but are close. These models have been excluded for M-m. Models marked with [1] can be ruled out because the observations indicate Si at high velocities incompatible with the chemical profiles. Note that the new delayed detonation models have not been included in this list. We found some evidence for a relation between the type of the explosion and of the host galaxy. In elliptical galaxies, SN Ia with shell-like structures are highly favored. These may be understood within the pulsating and merging scenarios. Because ellipticals consist on low mass stars only, this may provide a hint to the progenitor evolution; however, a larger sample of observations is needed to confirm this trend.

Supernovae	galaxy	Type	D[Mpc]	E_{B-V}	acceptable models
SN 1937C	IC 4182	Sm	4.5±1	0.10	N32,W7,DET2
SN 1970J	NGC 7619	dE	63 ± 8	0.01	DET2env2/4,(PDD3)
SN 1971G	NGC 4165	Sb	36 ± 9	0.04	M37, M36, W7,N32
SN 1972E	NGC 5253	I	4.0±0.6	0.04	M35,N21,M36,(HeD12[2])
SN 1972J	NGC 7634	SBO	52 ± 8	0.01	W7,M36/37,N32,DET2
SN 1973N	NGC 7495	Sc	69 ± 20	0.08	N32,M36,W7,(HeD10/11)
SN 1974G	NGC 4414	Sc	17.5 ± 5	0.0	N32,M36,W7,(HeD10/11)
SN 1975N	NGC 7723	SBO	28 ± 7	0.18:	PDD3/6/9/1a
SN 1981B	NGC 4536	Sb	19 ±4	0.05	M35, N21
SN 1983G	NGC 4753	S	15 ± 4	0.29	N32, W7 (M36)
SN 1984A	NGC 4419	Ep	16 ± 4	0.14	DET2env2, PDD3/6)
SN 1986G	NGC 5128	I	4.2±1.2	0.83	W7, N32, (M37/8)
SN 1988U	AC 118[1]	-	1440 ± 250	0.05	M36, W7, N32
SN 1989B	NGC 3627	Sb	8.7 ± 3	0.45	M37, M36
SN 1990N	NGC 4639	Sb	20 ± 5	0.05	DET2env2/4, PDD3/1a
SN 1990T	PGC 63925	Sa	180 ± 30	0.1	M37, M38
SN 1990Y	anonym.	E	195 ± 45	0.05	W7,N32,M36/37,PDD1c
SN 1990af	anonym.	E	265 ± 85	0.05	W7, N32, M36
SN 1991M	IC 1151	Sb	41 ± 10	0.12	M35, PDD3
SN 1991T	NGC 4527	Sb	12 ± 2	0.10	PDD3/6/1a. DET2env2
SN 1991bg	NGC 4374	dE	18 ± 5	0.25	PDD5/1c
SN 1992G	NGC 3294	Sc	29 ± 6	0.05	M36/35, PDD3, HeD10
SN 1992K	ESO269-G57	SBb	43^{+15}_{-8}	0.18	PDD5/1a,(M39,HeD2)
SN 1992bc	ESO-G9	S	83 ± 10	0.04	PDD6/3/1c
SN 1992bo	ESO-G57	S	79 ± 10	0.03	PDD8
SN 1994D	NGC 4526	S0	16 ± 2	0.00	M36, (W7, N32)

cases because its structure resembles those of DD models but it has some problems with the high velocities of Si lines in SN1994D (Höflich 1995).

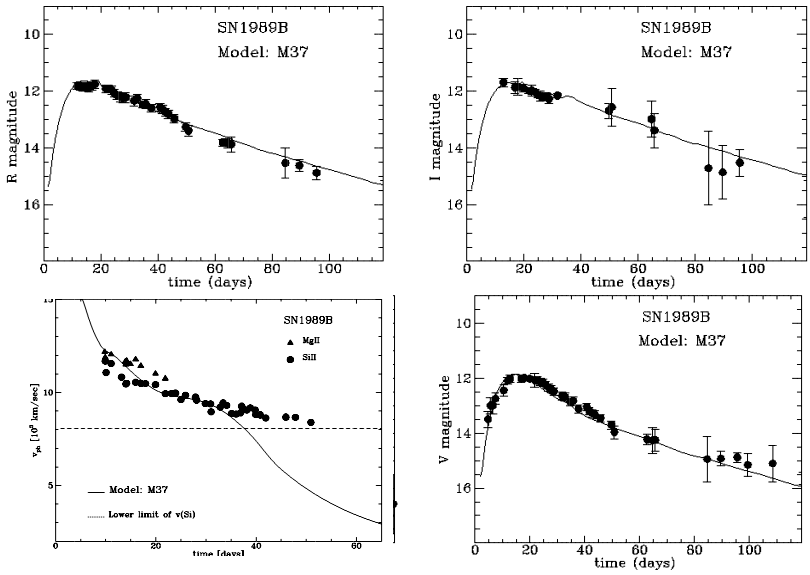

Figure 9. Monochromatic LCs of SN 1989B band compared with the calculated LC of the delayed detonation model M37. The 2 σ-error ranges are given by Wells et al. (1994). In the lower left plot, the photospheric velocity of the delayed detonation model M37 is given in comparison with the expansion velocities implied by the line shifts of Mg II and SiII. The dotted line is the velocity at which, in M37, the Si abundance has dropped to 10 % of its maximum value. The 'leveling off' of the line shift is produced by the chemical profile and not due to a change of the density profile. Note that detailed spectral synthesis is required to archieve a better accuracy or to test the ionization balance (Höflich 1995).

The "standard" explosion models are unable, however, to reproduce rise times to blue (visual) maximum longer than 15 days (17 days), provided the progenitor is a C/O WD of about 1.2 to $1.4 M_\odot$. In fact, slow rising and declining LCs have been observed (e.g. SN 1990N, SN 1991T) which require models with an envelope of typically 0.2 to $0.4 M_\odot$. The envelope can be produced during a strong pulsation or during the merging of two WD. The lower value should not be regarded as a physical limit, because it is likely that a continuous transition from models with and without an envelope exists. Note that a unique feature of models with massive envelopes are very high photospheric expansion velocities ($v_{ph} \approx 16,000$ km/s) shortly before maximum light, which drop rapidly to an almost constant value between 9000 and 12,000 km/s. This "plateau" in v_{ph} lasts for 1 to 2 weeks depending on the envelope mass (Khokhlov et al. 1993). In fact, there is some evidence for the plateau in v_{ph} from the Doppler shift of lines of SNe Ia with a slow pre-maximum rise and post-maximum decline (e.g. SN 1984A, SN 1990N, Müller & Höflich 1994).

Strongly subluminous supernovae (SN1991bg, SN1992K, SN1992bc) can

be explained within the framework of pulsating delayed detonation models with a low transition density. In particular, the models become systematically redder and the post-maximum decline becomes steeper with decreasing brightness in agreement with observations. However, we do not get unique relations between these different quantities. The evolution of the photospheric expansion velocity v_{ph} (Höflich et al. 1995) and, in particular, its steady decline, is consistent with observations. We must also note that we need a rather high intrinsic reddening for SN1992K and SN1991bg. Whether this can be explained by selective line blanketing, dust formation, or foreground clouds, or a combined effect is under investigation. The latter possibility must be regarded as unlikely, because, at later phases, the colors of these two supernovae are close to those of bright SNe Ia. Note that some of the 'classical' delayed detonation models (M39) also produce strongly subluminous LCs, but these do not fit any of the measurements.

Our Helium detonation models are rather unsuccessful in reproducing observations, mainly due to the rather steep post-maximum declines for normal bright supernovae, and Si lines observed at higher expansion velocities than compatible with the chemical profiles. At early times, our synthetic spectra are dominated by Fe-group elements and lack strong Si features because of the low abundances of Si ($\leq 10^{-2\ldots-3}$). For subluminous supernovae, the blue color at maximum light and the strong IR-maximum are both in contradiction to the observations. Quantitatively, multi-dimensional effects may alter the LCs mainly due to an increased escape probability for photons. However, the basic features of the LCs and spectra are not expected to change because they are inherent to the outer ^{56}Ni. The energy required to push the entire ^{56}Ni to sufficient high velocities ($\leq 16,000 km/sec$) is well in excess of the entire energy production.

Our findings with respect to the explosion scenario can be concluded as follows. Models with masses close to the Chandrasekhar limit provide the best agreement with the observations. Delayed-detonation and deflagration models similar to W7 and pulsation or merging scenarios are required. Based on the sparse observations, we cannot exclude the mechanism of Helium detonations. In particular, more early time spectra are crucial.

Pinto's group end up with a different result. Based on their calculations of the delayed detonation model DD4, they exclude this scenario. Their B and V LCs show rise times in excess of 21 days whereas both the U and bolometric LCs peak around day 15 and, at maximum light, their optical spectra show Co lines in strong emission (talk by R. Eastman). However, according to Pinto (priv. communication), their Helium detonations provide both excellent fits to spectra and LCs without encountering our Si problem. We find H_o to be $67 \pm 9 km/secMpc$ within a 95 % confidence level. This value agrees well with our previous analysis based on a subset of

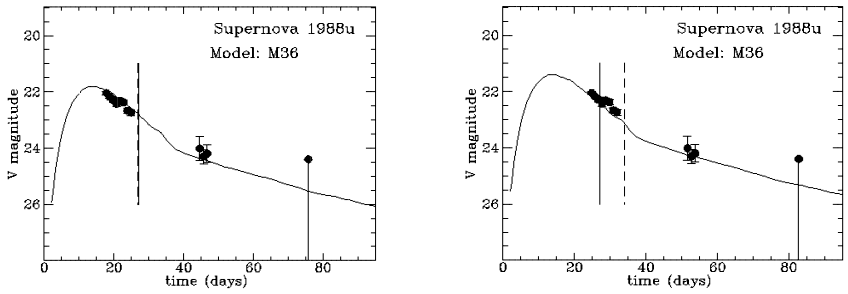

Figure 10. Visual LC of SN 1988U in comparison with the calculated LC of the delayed detonation model M36. Both the V and R colors are used. The dashed line marks the time when the photospheric velocity of the models corresponds to the observed line shift (thin line). The right and left plots correspond to different time shifts and both allow for a reasonable reproduction of the LC. This would correspond to an uncertainty of 0.5^m in the brightness. However, the right plot can be ruled out by the spectrum. This clearly demonstrates the importance of simultaneous analysis of both LCs and spectra.

observations and models ($66 \pm 10 km\ Mpc^{-1} sec^{-1}$, Müller & Höflich 1994). A strong variation of the local value can be ruled out at least on scales below 200 Mpc. From SN1988U, the deceleration parameter q_o is 0.7 ± 1.0 (2σ). Better limits can we expected in the near future when more and more distant SNeIa become available (Perlmutter et al. 1995).

6. Distance determinations, H_o and q_o

Based on our LCs, we have also determined the individual distances of the parent galaxies of the analyzed SNe Ia (Table 2). Our method does not rely on secondary distance indicators and allows for a consistent treatment of interstellar reddening and the interstellar redshift. The advantages of a consistent inclusion of information from the spectra becomes striking for SN1988U (Fig. 10).

Other determinations of H_o which are based on independent, purely statistical methods and primary distance indicators. It may be encouraging that the result of different SN Ia based methods agree if SN Ia are not treated as as standard candles. Hamuy et al. (1995) found 65 ± 5, Riess et al. (1995) give 67 ± 5, and Fisher et al. (1995), Nugent et al. (1995b) and Branch et al, (1995) get a values of 60 ± 10, 60 ± 12 and 58 ± 7, respectively. From our models, both the empirical relations between $M_V/dM(15)$ like-relations and the ansatz to deselect subluminous SNeIa seems to be justified, but we expect an individual dispersion of $\approx 20\%$ (Hamuy et al. 1995b).

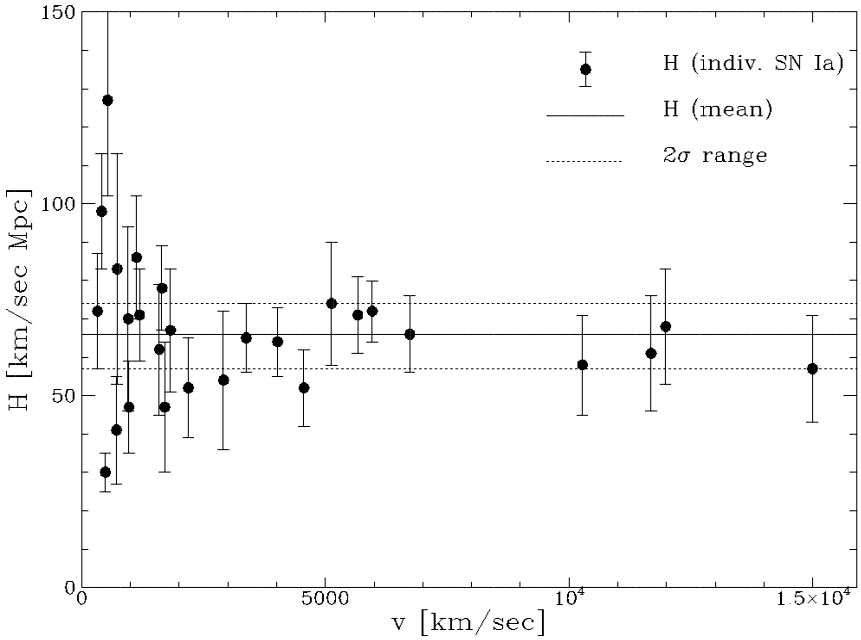

Figure 11. Hubble values H are shown based on individual distances (see table 2). SN1988U at v=91500 km/sec gives $H = 64 \pm 10$ [km/sec Mpc].

7. References

Arnett, W.D., Branch D., Wheeler J.C. (1985), *Nature*, **314**, 337
Arnett, W.D. (1969), *ApJS*,**5**, 180
Athay R., (1972), Radiation Transport in Spectral Lines, Dordrecht, D.Reidel Publ.Comp.
Ayres T., Wiedemann G.R. (1989), *ApJ*, **338**, 1033
Barbon R., Bennetti S., CApJalaro E., Rosino L., Turatto M. (1990), *A&A*, **237**, 79
Bessel, M., (1990),*PASP*, **102**, 1181
Branch D., et al. (1995), *Phys. Rep.*, submitted
Canal R. (1995),Les Houches Lectures, eds. J. Audouze et al., Elsevier, in press
Castor, J.I. (1974), *MNRAS*, **169**, 279
Collela P., Woodward P.R. (1984),*J. Comp. Phys.*, **54**, 174
Filippenko A.V. et al. (1992), *AJ*, **104**, 1543
Fisher A., Branch D., Höflich P., Khokhlov A., Wheeler J.C, (1995), *ApJ*, **447L**, 731
Frogel J.A. et al. (1987), *ApJ*, **315L**, 129
Hachisu I., Eriguchi Y., Nomoto K. (1986b), *A&A*, **168**, 130
Hamuy M. et al. (1994), *AJ*, **108**, 2226
Hamuy M. et al. (1995), *AJ*, **109**, 1
Hamuy M., Höflich P., Khokhlov A., Wheeler J.C. (1995b), *ApJ*, accepted
Hansen, C.J., Wheeler, J.C. (1969) *ApJSS*, **3**, 464
Harkness, R.P. (1991), in: SN1987A, ed. I.J. Danziger, ESO, Garching, p.447

Höflich, P., (1990), Habilitation thesis, U. of Munich, MPA 563
Höflich, P., Khokhlov, A., Müller, E. (1991),*A&A*,**248**, L7
Höflich, P., Müller, E,; Khokhlov, A. (1993), *A&A*, **268**, 570
Höflich P., Khokhlov A. (1995), **ApJ**, in press
Höflich P., Khokhlov A., Wheeler C. (1995), *ApJ*, **444**, 831
Hoyle P., Fowler , (1960) *ApJ*, **132**. 565
Iben, I.Jr., Tutukov, A.V. (1984), *ApJS*, **54**, 335
Jeffery D. (1995), *A& A*, **299**, 770
Khokhlov A., Müller E., Höflich P. (1993), *A&A*, **270**, 23
Khokhlov A., (1991ab), *A&A*, **245**, 114 & L25
Leibundgut, B. et al., (1993), *AJ*, **105**, 301
Karp, A.H., Lasher, G., Chan, K.L., Salpeter E.E., 1977, *ApJ* , **214**, 161
Kurucz, R. (1993),Atomic Data for Opacity Calculations, Cambridge, CfA
Livne E., Arnett D. (1995), *ApJ*, in press
Mihalas, D. (1978), Stellar Atmospheres, Freeman, San Francisco
Mihalas D., Kunasz R.B., Hummer D.G. (1975), *ApJ*, **202**, 465
Mihalas D., Kunasz R.B., Hummer D.G. (1976), *ApJ*, **206**, 515
Mihalas D., Kunasz R.B., Hummer D.G. (1976b), *ApJ*, **210**, 419
Müller E., Höflich P., (1994), *A&A*, **281**, 51
Nomoto K., Yamaoka H., Shigeyama T., Iwamoto K., (1995), *in: Supernovae*, ed. R.A. McCray, Cambridge University Press, in press
Nomoto K., Thielemann F.-K., Yokoi K. (1984), *ApJ*, **286**, 644
Nomoto K., Sugimoto D., (1977), *PASJ*, **29**, 765
Nomoto K. (1982), *ApJ*, **253**, 798
Nomoto, K., Sugimoto, D., Neo, S. (1976) *ApJSS*, **39**, 137
Nugent P., Baron E.,Hauschild P., Branch D. (1995a), *ApJ*, **441L**, 33
Nugent P., et al. (1995b), *Phys. Rev. Let.*, **75**, 394 & 1974(E)
Olsson G.L., Auer L.H., Buchler J.R. (1986), *JQSRT*, **35**, 431
Perlmutter et al. (1995), *ApJ*, **440L**, 41
Phillips M.M. et al.(1987), *PASP*, **90**, 592
Pskovskii Yu.P., (1970), *Astron. Zh.*, **47**, 994
Riess A.G., Press W.H., Kirshner R.P., (1995), *ApJ*, **438L**, 17
Ruiz-Lapuente P. et al. , (1993), *Nature*, **365**, 728
Rybicki G.B., Press W.H. (1995), *Phys.Rev.Let.*, in press
Shigeyama T. et al (1993), *AAS*, **97**, 223
Thielemann F.-K. et al. (1994), in: Supernovae, Elsevier, Amsterdam, 629
Thielemann F.-K., Arnould M., Truran J.W., (1987), Advances in Nuclear Astrophysics, E. Vangioni-FlamEditions frontières, Gif sur Yvette, 525
Wells, L.A. et al. (1994), *AJ*, **108**, 2233
Wheeler J. C., Harkness R .P., (1990), *Rep. Prog. Phys.*, **53**, 1467
Wheeler J. C., Harkness R .P., Khokhlov A., Höflich P., (1995), *Phys.Rep.*, in press
Woosley S. E., Weaver T. A. (1994), in: Supernovae, Elsevier, Amsterdam, 423
Woosley S. E. & Weaver, T. A. (1994), *ApJ*, **423**, 371
Yamaoka H., Nomoto K., Shigeyama T., Thielemann F. (1992), *A&A*, **393**, 55

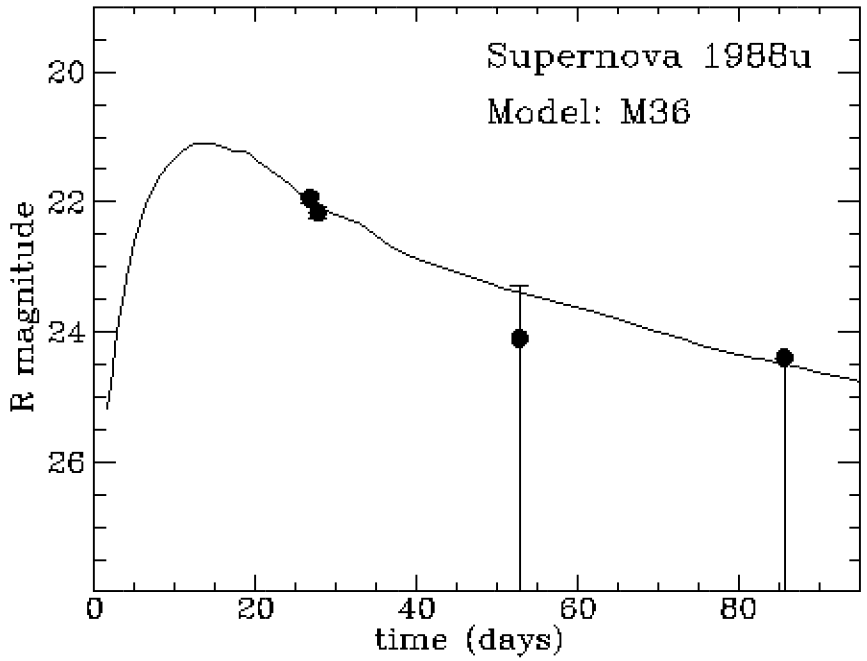
Supernova 1988u
Model: M36
R magnitude
20
22
24
26
0
20
40
60
80
time (days)

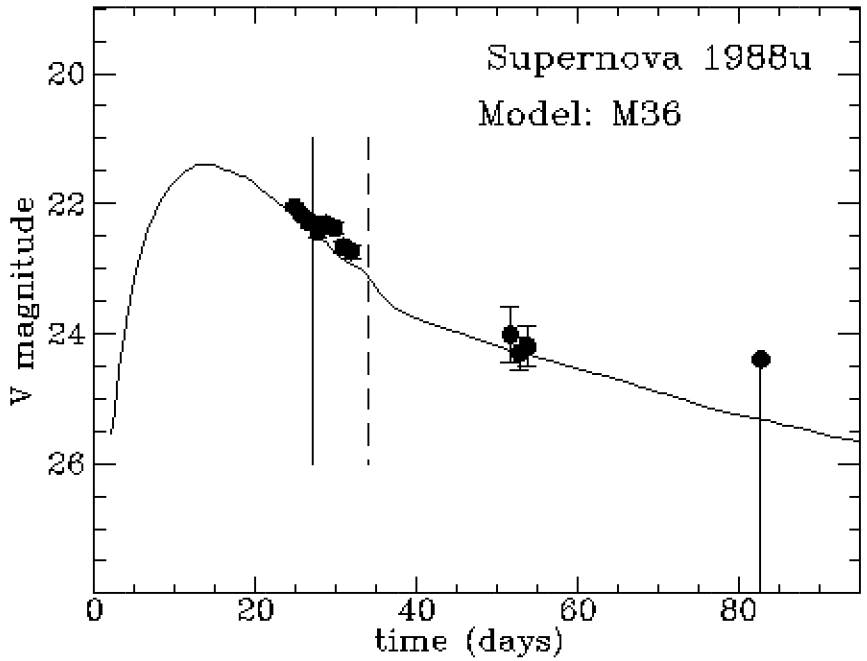
Supernova 1988u
Model: M36
V magnitude
20
22
24
26
0
20
40
60
80
time (days)

Abundances

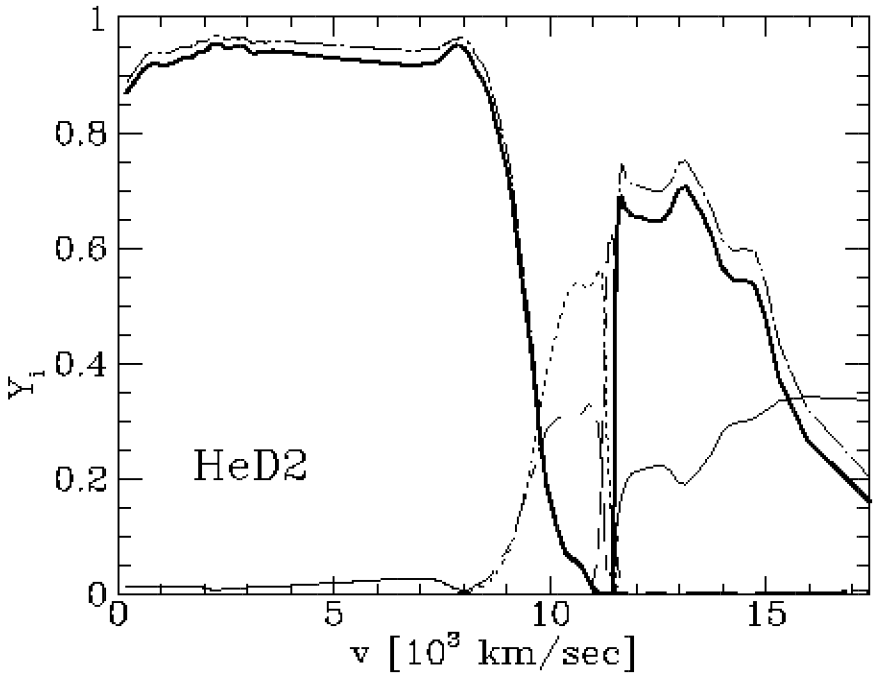
HeD2
Y_i
v [10^3 km/sec]

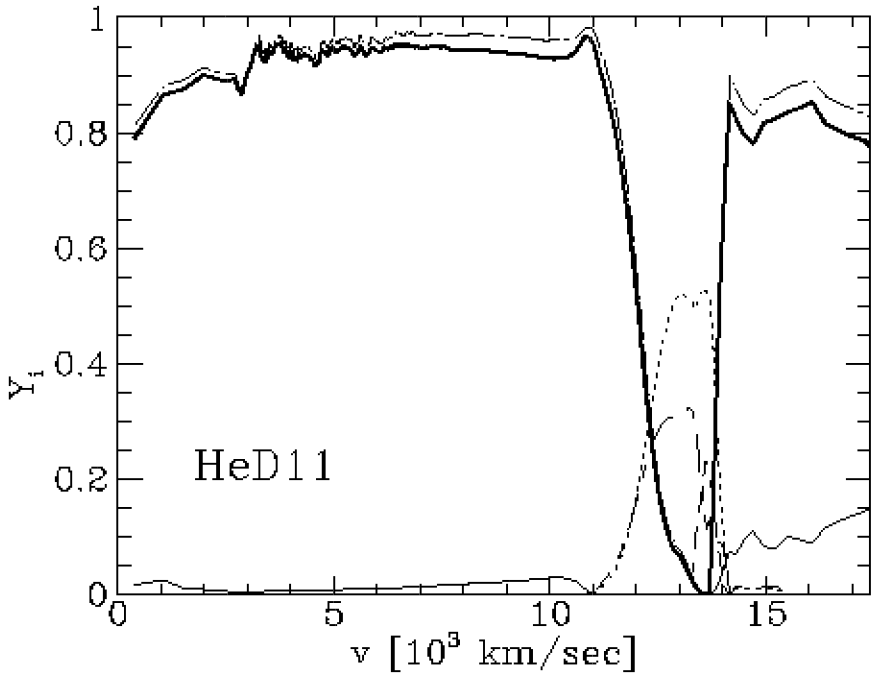
HeD11
Y_i
v [10^3 km/sec]

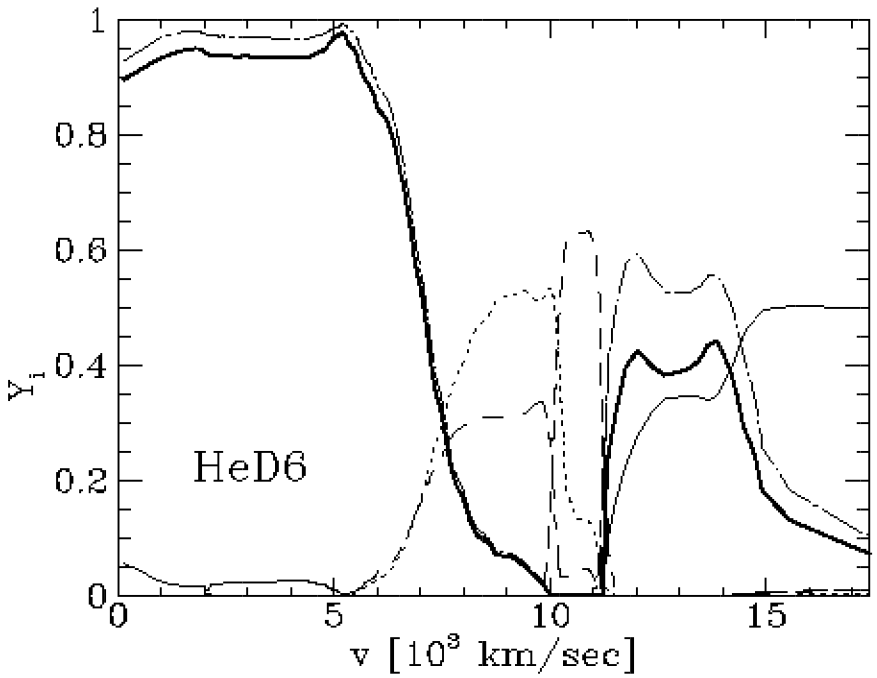
HeD6
Y_i
v [10^3 km/sec]

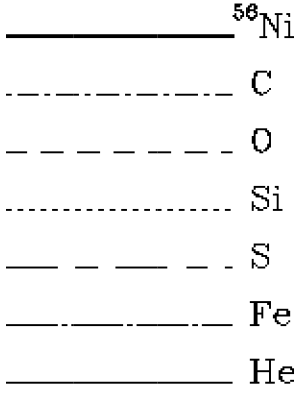
^{56}Ni
C
O
Si
S
Fe
He

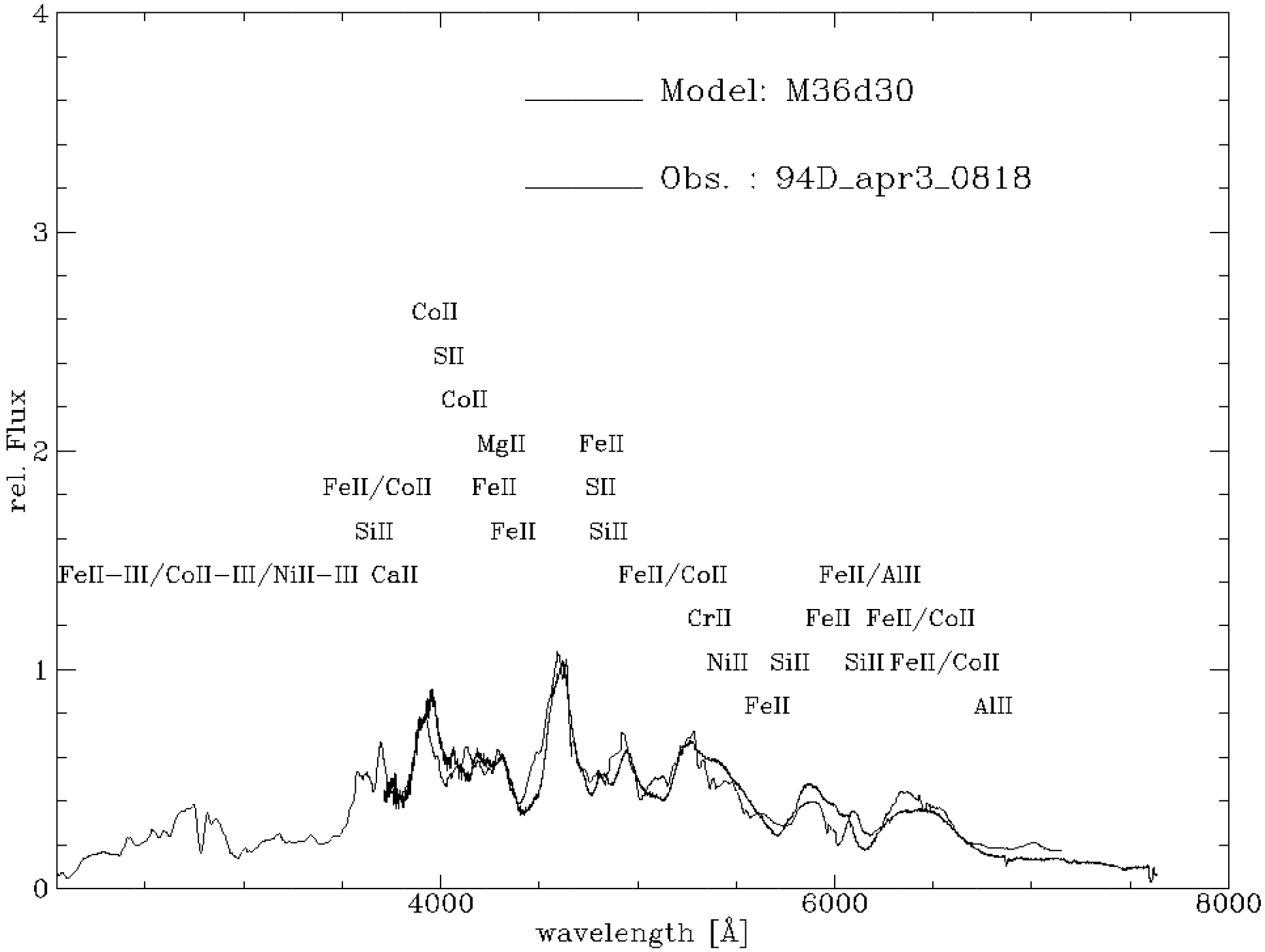
Model: M36d30
Obs. : 94D_apr3_0818
CoII
SII
CoII
MgII
FeII
FeII/CoII
FeII
SII
SiII
FeII
SiII
FeII−III/CoII−III/NiII−III
CaII
FeII/CoII
FeII/AlII
CrII
FeII
FeII/CoII
NiII
SiII
SiII
FeII/CoII
FeII
AlII
rel. Flux
wavelength [Å]
0
1
2
3
4
4000
6000
8000